K–Ar age of the Ranau Tuffs: Implications for the Ranau caldera emplacement and slip-partitioning in Sumatra…

Article *in* Tectonophysics · November 1999

DOI: 10.1016/S0040-1951(99)00198-5

CITATIONS
36

READS
180

5 authors, including:

Olivier Bellier
Centre Européen de Recherche et d'En…
199 PUBLICATIONS **3,241** CITATIONS
SEE PROFILE

Hervé Bellon
Université de Bretagne Occidentale
321 PUBLICATIONS **7,860** CITATIONS
SEE PROFILE

Michel Sébrier
Pierre and Marie Curie University - Paris 6
129 PUBLICATIONS **2,503** CITATIONS
SEE PROFILE

René C Maury
Université de Bretagne Occidentale
346 PUBLICATIONS **10,475** CITATIONS
SEE PROFILE

Available online at www.sciencedirect.com
SCIENCE DIRECT
Tectonophysics 413 (2006) 201–220
TECTONOPHYSICS
www.elsevier.com/locate/tecto

Fission track and fault kinematics analyses for new insight into the Late Cenozoic tectonic regime changes in West-Central Sulawesi (Indonesia)

Olivier Bellier [a,*], Michel Sébrier [b], Diane Seward [c], Thierry Beaudouin [d], Michel Villeneuve [e], Eka Putranto [f]

[a] *UMR CNRS 6635- CEREGE (Centre Européen de Recherche et d'Enseignement des Géosciences de l'Environnement), Université Paul Cézanne Aix-Marseille, BP 80, Europôle Méditerranéen de l'Arbois, 13545 Aix en Provence Cedex 4, France*
[b] *UMR CNRS 7072 "Tectonique", Université Pierre et Marie Curie, T26-E1, case 129, 4, place Jussieu, 75252, Paris cedex 05, France*
[c] *Geology Institute, ETH- Zürich, Sonneggstrasse 5, 8092 Zürich, Switzerland*
[d] *UMR CNRS 8616 "ORSAYTERRE", Université de Paris-Sud, 91405 Orsay Cedex, France*
[e] *URA-CNRS 1208, Univ. de Provence, Marseille, France*
[f] *DGGMR/PPPG (Geological Research and Development Centre), Bandung, Indonesia*

Received 24 March 2005; received in revised form 18 August 2005; accepted 24 October 2005
Available online 10 January 2006

Abstract

The left-lateral strike-slip Central Sulawesi Fault System (CSFS, composed of the NNW Palu–Koro (PKF) and the ESE Matano faults) is located within the eastern Indonesian triple junction between the Pacific, Indo-Australian and Eurasian plates. Fault kinematic and fission-track analyses show that the Late Cenozoic central Sulawesi deformation results from three successive tectonic regimes: (1) A Late Miocene–early Pliocene (5 Ma) WNW-trending shortening characterized by transpressional deformation along the PKF and compressional in the Poso area. This tectonics resulted from the collision between the Banggai–Sula block with Sulawesi. It produced locally a transpressional regime as a consequence of the northward extrusion of the Central Sulawesi block limited by the PKF. (2) A Pliocene collapse tectonic regime associated with W-trending extension. Coeval with these events regional cooling and exhumation took place. (3) A Quaternary transtensional regime resulting from the combined effects of the Central Sulawesi block northward motion, and extension related to back-arc spreading behind the North Sulawesi subduction (Tomini Gulf).

1. Introduction

Sulawesi Island, eastern Indonesia, is located at the junction between the converging Pacific-Philippine, Indo-Australian Plates and the Sundaland, i.e. the south-eastern part of the Eurasian Plate (Fig. 1). Sulawesi tectonic evolution results from successive collisions of continental slivers, island arcs, and oceanic domains with the Sundaland. The Central Sulawesi Fault System (CSFS), one of the major structures in SE Asia, cuts across Sulawesi Island from NW to SE, connecting the North Sulawesi subduction zone to the Banda Sea deformation zones (Fig. 1). Seismicity of Sulawesi as recorded by global seismic networks, as well as local Indonesian networks and historic data,

* Corresponding author.
E-mail address: bellier@cerege.fr (O. Bellier).

0040-1951/$ - see front matter © 2005 Elsevier B.V. All rights reserved.
doi:10.1016/j.tecto.2005.10.036

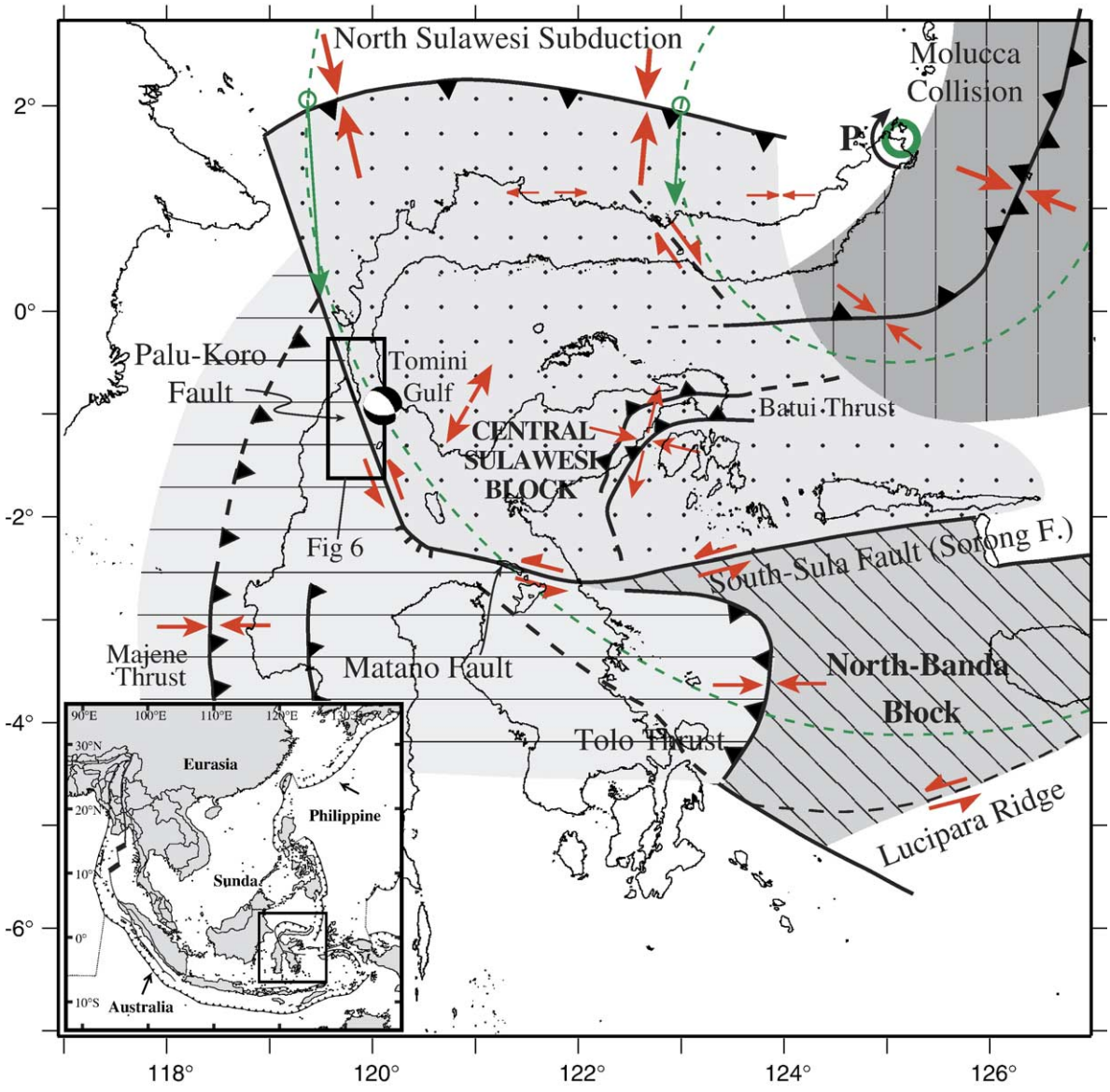

Fig. 1. Regional geodynamic sketch that presents the present day deformation model of Sulawesi area (after Beaudouin et al., 2003) and four main deformation systems around the Central Sulawesi block, highlighting the tectonic complexity of Sulawesi. Approximate location of the Central Sulawesi block rotation pole (P) [compatible with both GPS measurements (Walpersdorf et al., 1998a) and earthquake moment tensor analyses (Beaudouin et al., 2003)], as well as the major active structures are reported. Central Sulawesi Fault System (CSFS) is formed by the Palu–Koro and Matano faults. Arrows correspond to the compression and/or extension directions deduced from both inversion and moment tensor analyses of the focal mechanisms; arrow size being proportional to the deformation rate (e.g., Beaudouin et al., 2003). We also represent the focal mechanism provided by the Harvard CMT database [CMT data base, 2005] for the recent large earthquake (M_w=6.2; 2005/1/23; lat.=0.92°S; long.=120.10°E). The box indicates the approximate location of the Fig. 6 that corresponds to the geological map of the Palu basin region. The bottom inset shows the SE Asia and Sulawesi geodynamic frame where arrows represent the approximate Indo-Australian and Philippines plate motions relative to Eurasia.

indicate low shallow depth activity in Central Sulawesi (e.g., Katili, 1970; Bellier et al., 1998; Beaudouin et al., 2003). However, previous studies have shown evidence for major present-day tectonic activity along the CSFS (Tjia, 1981; Hamilton, 1979; Silver et al., 1983; Bellier et al., 2001). Indeed, the long-term slip rate of the CSFS was indirectly estimated at about 30–50 mm/yr for the last 5 Myr, from plate kinematics (e.g., Silver et al., 1983; Walpersdorf et al., 1998a) and paleomagnetic studies (Surmont et al., 1994). Recently, several complementary approaches (GPS measurements, geomorphic and tectonic studies) have con-

firmed this high level of activity (e.g., Walpersdorf et al., 1998b; Stevens et al., 1999; Bellier et al., 2001; Vigny et al., 2002). In order to integrate these high deformation rates within both the Sulawesi geodynamic framework and the Late Cenozoic tectonic evolution in central Sulawesi, fault kinematics and fission-track analyses have been conducted. These analyses provide evidence for drastic changes in the Late Cenozoic tectonic regime and for a rapid and significant cooling and exhumation of central Sulawesi in the Pliocene consequent to the last major collision phase affecting Sulawesi.

2. Geodynamic framework, seismicity, and present-day stress regime acting around Sulawesi

Localised at a major plate junction, Sulawesi Island's peculiar shape results from an on-going, complex history of collisions and rotations of continental slivers, island arcs, and oceanic domains with the Sundaland (Fig. 1). These collisional blocks originated from both the Philippine-Pacific and the Indo-Australian regions, in a process which has been on-going since Cretaceous times (Katili, 1975; Hamilton, 1979; Rangin, 1989; Daly et al., 1991; Hall, 1996, 2002). A summary from recent studies (e.g., Polvé et al., 1997, 2001; Villeneuve et al., 2000; Elburg et al., 2003; Calvert and Hall, 2003; Van Leeuwen and Muhardjo, 2005) permits us to propose a reappraisal for the SE Asian geodynamic reconstruction resulting in successive Sulawesian Late Cenozoic tectonic stages. During *Early Miocene*, a microcontinental fragment from Australia collided with SE Sulawesi as testified by ophiolites. Subsequently to this collision, during the *Middle–Upper Miocene* a metamorphic core complex developed in Sulawesi within a regional extension phase that brought about the development of several basins within the Banda area. Initiated in the early Pliocene a final collision occurred in Sulawesi, between the Sulawesi East arm and the Irian-Jaya-derived Baggai–Sula block, at about 5 Ma (Hall and Wilson, 2000; Hall, 2002). It is identified by the occurrence of an ophiolite belt in the East arm of the island (Villeneuve et al., 2000), uplift, folding and thrusting in Central-Western Sulawesi, and by inversion of Paleogene grabens (Van Leeuwen and Muhardjo, 2005). This event produced in Western Sulawesi, west-verging thrusting and folding (Bergman et al., 1996) and the development of the NNW-trending Palu–Koro strike-slip Fault (PKF) that melted part of the lower crust (e.g., Polvé et al., 2001), a rapid uplift of mountains of about 2.5 km, and deposition of syn- to post-orogenic sediments such as Late Pliocene molasse sedimentation around the early Pliocene collision zones.

Seismic networks document a high level of seismicity in the northern boundaries, corresponding to the deformation along the North Sulawesi trench and within the Molucca Sea subduction zone (Beaudouin et al., 2003). Seismic activity is less in central and south Sulawesi; it represents the activity of the East, South and SE arms' thrusts and the left-lateral CSFS. Silver et al. (1983) proposed a deformation model that implies a clockwise rotation of the Central Sulawesi block that is limited to the west and south by the CSFS (the term Central Sulawesi block in this manuscript includes the North Sulawesi arm bounded by the North Sulawesi trench, to the north, the PKF, to the west, and the Matano fault to the south). Paleomagnetic (Surmont et al., 1994), geodetic (Walpersdorf et al., 1998a) and seismologic (Beaudouin et al., 2003) studies confirm and define this rotation (Fig. 1). To better understand the present-day kinematics and deformation of Sulawesi area, Beaudouin et al. (2003) performed a seismotectonic study, using focal mechanism data of moderate and large (M_w=5) shallow earthquakes (=60 km). These focal solutions were analysed by inversion and moment tensor summations, in order to obtain stress state deviators as well as tensors and rate estimates of the present-day deformation (Fig. 1). Along the North-Sulawesi subduction zone, directions of the stress axes are not significantly different from east to west (σ_1: N356 ± 5°E), but the calculated slip rate increases from 20 ± 4 to 54 ± 10 mm/yr, respectively. These values agree with the Central Sulawesi block rotation pole previously proposed and located at the eastern extremity of the northern arm (Fig. 1). The CSFS that bounds the Central Sulawesi block plays a major role within this rotation. However, seismicity documents few moderate magnitude earthquakes related to the left-lateral CSFS, despite the many active tectonic features (Beaudouin, 1998; Bellier et al., 2001). A recent large earthquake (M_w=6.2; 2005/1/23; lat.=0.92°S; long.=120.10°E) recorded by global seismic networks highlights the activity of the present day kinematics of the northern CSFS. The focal mechanism provided by the Harvard CMT database (Fig. 1) gives evidence for a N321°E-trending (for a dip of 55°E) focal plane (CMT data base, 2005), relatively consistent with the regional orientation of the structures. In addition, this focal mechanism suggests transtensional deformation acting close to the PKF study area, i.e. normal faulting with a left-lateral strike-slip component.

The southeastern limit of the Central Sulawesi block is represented by ENE-trending Sorong strike-slip fault that extends from Irian-Jaya Island to the east coast of

Sulawesi, where it connects to the CSFS (i.e., to the Matano fault) through the South Sula fault (e.g., Hinschberger et al., 2000; Beaudouin et al., 2003). The inversion provides a strike-slip regime with a NE-trending σ_1 stress axis, for this region. Beaudouin et al. (2003) highlight the Central Sulawesi block internal deformation that could explain residuals in the GPS velocities obtained by Walpersdorf et al. (1998a) within the modelling of the Central Sulawesi block rotation. This deformation corresponds to a NE-trending extensional stress regime in the southern Tomini Gulf zone at a rate of 9 mm/yr (Fig. 1). The Batui zone that corresponds to the Pliocene collision zone between the East arm and the Banggai–Sula block is presently affected by strike-slip earthquakes. The South arm of Sulawesi is affected by a N100°E-trending compression involving the Majene–Kalosi thrust system. This is related to a N80°E-trending convergence rate of 8.5 mm/yr, while the Tolo thrust, lying off the SE arm east coast, absorbs the subduction to the west of the North Banda Sea, as shown by moderate earthquakes with reverse faulting focal mechanisms.

3. The Central Sulawesi active deformation

A large-scale active fault map covering central Sulawesi was compiled by investigation of detailed geomorphic fault characteristics using SPOT images (e.g., Bellier et al., 1998, 2001; Beaudouin, 1998). This image analysis has been further constrained by structural field studies and complemented by a geomorphic study on topographic and geological maps (G.R.D.C., 1981 to 1993). This map provides evidence for 3 distinct deformation domains (Fig. 2): the CSFS, the SE arm fault zones and the Poso fault zone (bounding the Poso Lake).

The major active fault system in Sulawesi is the CSFS. It connects, from northwest to southeast, the North Sulawesi Subduction to the Tolo Thrust and Sorong Fault, in the North Banda Sea. The CSFS mainly corresponds to two active fault zones that displaced geomorphic features and thus accounts for the major active deformation in central Sulawesi. The NNW-trending PKF, in the west, and the W–WNW-trending Matano Fault, in east-central Sulawesi (Fig. 2) are connected by a broad geometric discontinuity that is arranged in a complex crustal releasing fault bend, the Leboni releasing fault zone, located at around 2°15'S (Leboni RFZ on Fig. 2).

To examine potential partitioning of the deformation across the Palu–Koro and Matano regions, detailed mapping of the Quaternary surface fault traces was conducted. The geomorphic characteristics of these faults provide evidence for strong recent activity (Bellier et al., 1998, 2001). Their traces are clear and horizontal stream offsets, and alluvial fan asymmetries are visible. The tectonic activity of the northernmost segment of the CSFS, has been studied by detailed mapping of the Quaternary surface fault traces and of the offsets along the fault strike (Bellier et al., 2001) allowing a compilation of a PKF segmentation map. This map shows that the southern PKF fault trace is particularly well expressed along the Palu–Koro valley and is characterised by localised deformation on long straight segments. Conversely, the northernmost (onshore) PKF comprises several smaller segments arranged in an en echelon pattern, indicating a growing complexity in the segmentation as one progresses northwards. In the northernmost zone, the deformation is probably distributed over a broad zone and extends into the Palu Gulf offshore domain.

While in eastern Sulawesi island, the faults are distributed over three fault zones, in the east-central Sulawesi and SE arm of Sulawesi the active deformation mainly occurred on the W- to WNW-trending Matano Fault, that runs from the Leboni releasing fault zone, at the west, to the Losoni Bay to the east. Geomorphic characteristics, narrow and steep valleys, ridges and horizontal stream offsets, suggest a high level of activity along this 200-km long fault. In addition, it displaces left-laterally East Sulawesi ophiolites by about 25 km. The 30 by 7.5 km Matano Lake elongated along an about N110°E-strike represents a pull-apart basin that connects two major domains of the Matano Fault. This lake is bounded to the north and south by 350 and 900 m-high escarpments, respectively, while its depth is about 600 m. These morphologic characteristics suggest that this basin is actively subsiding. At 20 km west of this pull-apart, at about 121°10′E, a subsiding relay zone corresponds to a domain where the faults splay. Indeed, this discontinuity is the domain connection with several WNW- to NW-trending faults — the major one being the Lawanopo Fault which trends about N145 ± 10°E and obliquely cross-cuts the SE arm of Sulawesi. Another major NW-trending fault, partly bounding the Bone Gulf, affects the SE arm of Sulawesi. It is the Mendoke Fault that may have been the southern continuation of the PKF in Late Tertiary–Early Pleistocene (?) and contributed to the counter-clockwise rotation of the Sulawesi SE arm that accompanied the Bone Gulf opening. However, geomorphic characteristics of the both Lawanopo and Mendoke faults seem to indicate that they are presently inactive or poorly active (discontinued and eroded fault traces...). East of the PKF

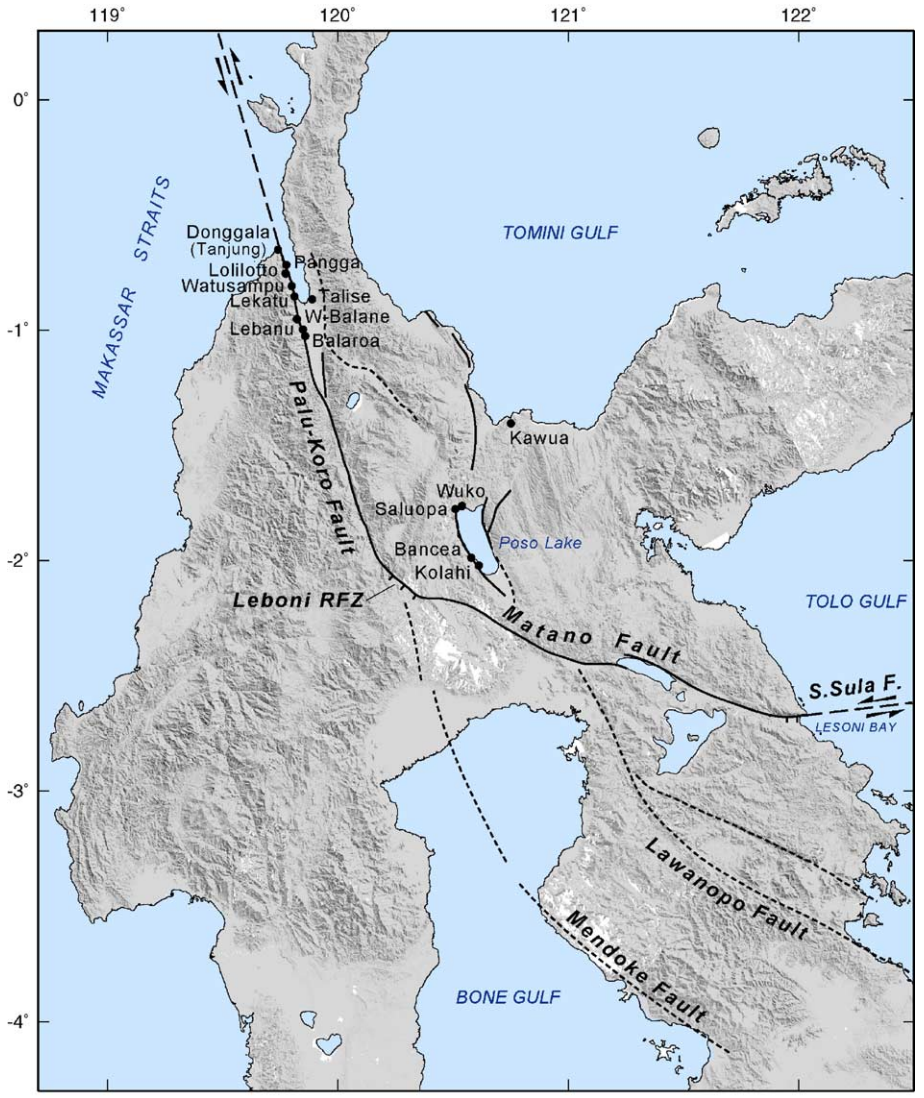

Fig. 2. Sketch map of the Cenozoic Central Sulawesi fault system. ML represents the Matano Lake, and Leboni RFZ, the Leboni releasing fault zone that connects the Palu–Koro and Matano Faults. Triangles indicate faults with reverse component (triangles on the upthrown block). On this map are reported the fault kinematic measurement sites (geographic coordinates in Table 3).

zone, the intra-mountain domain is characterised by the occurrence of several Quaternary depressions (Poso, Palolo, Gintu, Lindu basins…), partly bounded by fault escarpments and thus probably tectonically controlled during their subsidence. The N160°E-trending Poso basin is the most prominent. The Poso NNW-striking 400 m-deep lake lies within part of this basin. Its western edge is marked by right-stepping NNE-trending en echelon arranged fault escarpments while the eastern bank is affected by oblique NNE-trending as well as parallel NNW-trending faults. Discontinuous faults seem to connect the basin faults northward to the Tomini Gulf. These faults, including the basin boundary faults, do not provide evidence for clear present-day activity, however they seem to control the NE-striking depression within the southern Tomini Gulf (e.g., Beaudouin, 1998).

4. Geomorphic evidence for the PKF present-day fault kinematics and Cenozoic tectonic regime change

The northernmost segments of the PKF appear geomorphically more active and bound the western part of the Palu basin (location Fig. 1). This is an asymmetric basin bounded to the east by an inactive or almost

inactive (i.e., characterised by no active displacement or slow slip rate) fault. The PKF segments exhibit left-lateral offsets of geomorphic features (e.g., Bellier et al., 2001); i.e. streams, late Quaternary alluvial fans (Fig. 3), shutter ridges, etc. The western Palu basin boundary front is controlled by a N- to NNW-trending, about 2300 m high escarpment locally incised by wine-glass valleys, the base of which is marked by faceted spurs with 300–400 m high triangular facets (Fig. 4). The geomorphic characteristics of this escarpment that represents the northern PKF trace, as well as Quaternary coral reef terraces uplifted by 210 m (Tjia and Zakaria, 1974; Beaudouin, 1998), indicate that a normal slip component characterises the PKF present-day faulting. In addition, field observations show that the wine-glass stem of the wine-glass valleys are left-laterally bent (Fig. 4) suggesting a combined vertical (normal) and lateral displacement for the PKF present-day activity.

Consequently, these general geomorphic characteristics indicate both combined strike-slip and normal-slip faulting presently occurring along the northern PKF. This supports the interpretation of GPS measurements (e.g., Walpersdorf et al., 1998b) suggesting a transtensional regime. Similarly, the analysis of the slip-vectors measured on the major fault planes affecting recent deposits confirms this tectonic regime (see following section on fault kinematics). The major faults bounding the basin are marked by numerous scarps with faceted spurs; the base of the faceted spurs being locally marked by a several meters-high scarp. Analysis of SPOT images, coupled with field observations and topographic profiles indicate two generations of faceted spurs. Indeed, the 2300 m high escarpment that bounds the Palu basin western edge is characterised by two distinct slope angles (Figs. 4 and 5A). The youngest faceted spurs are marked by triangular facet with a mean slope of about $35 \pm 5°$E, while older spurs, incised by wine-glass valleys (Fig. 4) are characterised by a mean escarpment slope of $20 \pm 5°$E. This escarpment slope change is underlain by local benches that could represent a quiescent uplift period. These distinct sets of faceted spurs must have formed during periods when

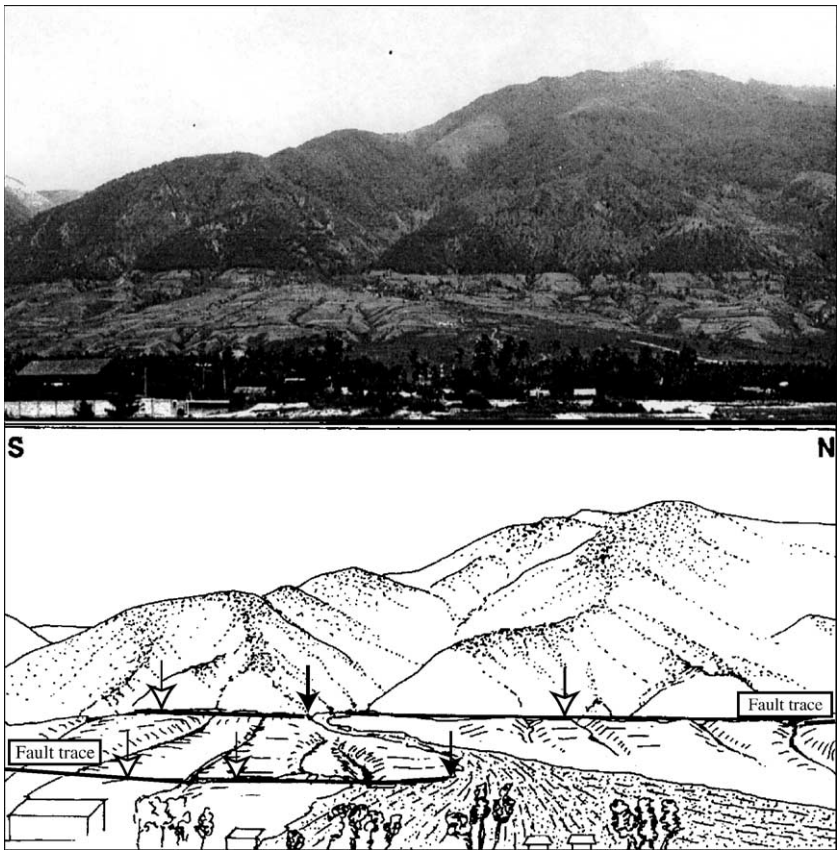

Fig. 3. West-looking view of the Palu–Koro fault escarpment SSW of the Palu basin showing faceted spurs and a left-lateral offset of an alluvial fan. At the bottom, sketch of the photograph where white arrows point to the fault trace and black arrows point to the cumulate fan offset along the fault traces.

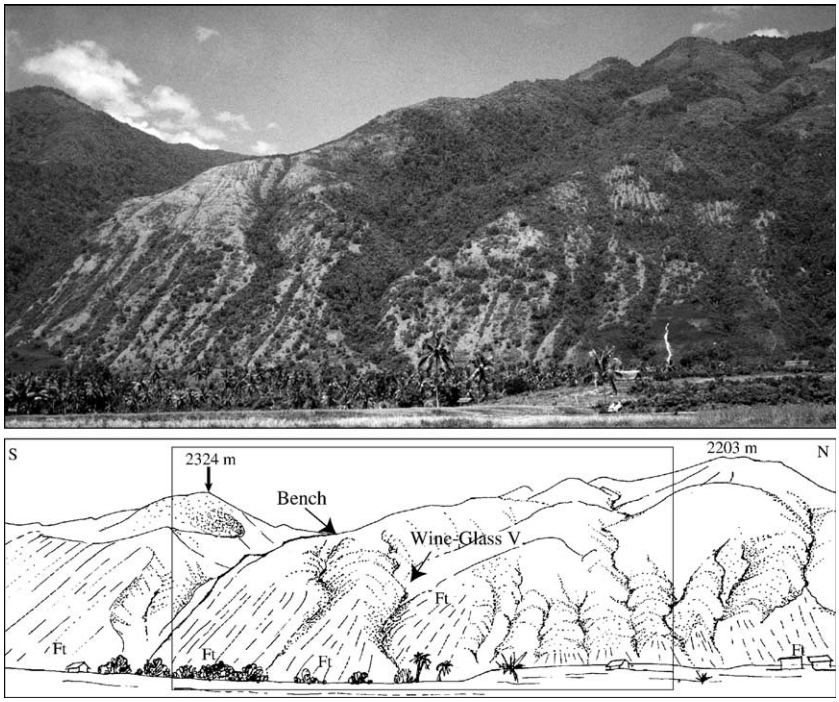

Fig. 4. South-west-looking view of the Palu–Koro fault escarpment at SSW of the Palu basin. At the bottom a sketch of the Palu–Koro fault escarpment (box bound the above view), where are represented the triangular facets (Ft), benches and a win-glass valley.

the fault displacement was faster than the recession of the fault scarp due to the erosion (e.g., Hamblin, 1976; Zhang et al., 1998). This geomorphic feature suggests that the western Palu basin escarpment is inherited from several uplift stages and consequently its formation has been controlled by distinct phases of deformation (for

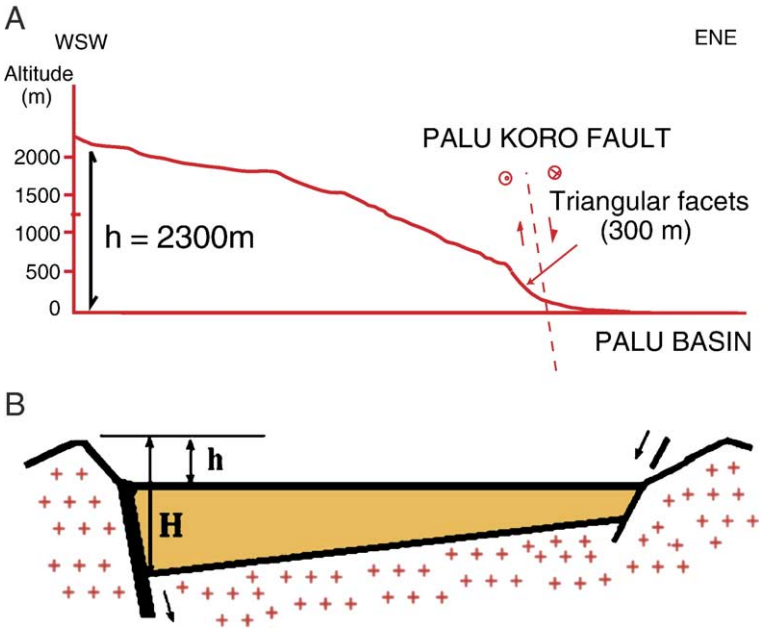

Fig. 5. WSW-trending topographic section of the western border fault escarpment Palu Palu basin. At the bottom (B), we represent a sketch of the Palu basin showing the relationship between the escarpment high (h) and the total vertical component (H) of the fault displacement (for more details see the text).

escarpment morphology history recorded by different generations of faceted spurs, see for example Zhang et al., 1998). This escarpment polygenesis is clearly confirmed by fault kinematics analyses presented in the current study that indicate several recent phases of deformation in the study zone.

5. PKF left-lateral slip rate estimates

We report the available estimates of the PKF lateral slip rates that are calculated for different time scales (see Table 1). The slip rate of the PKF has been previously indirectly estimated from plate convergence velocity along the North Sulawesi subduction and by paleomagnetic studies. Assuming that the strike-slip motion along the PKF could accommodate the total normal-to-the-trench component of the convergence off the North Sulawesi subduction, between the Celebes Sea plate, and the central Sulawesi block, the theoretical maximum slip rate of the PKF has been estimated to be about 50 mm/yr. It has accommodated 250 km in the last 5 My (Silver et al., 1983). The other indirect estimate deduced from paleomagnetic studies suggests that the about -20° clockwise rotation of the Sulawesi northern arm has occurred since late Miocene, i.e. during the last 5 My (Surmont et al., 1994). This suggests about 150 km of left-lateral displacement along the PKF that corresponds to an about 30 mm/yr slip rate. This long-term slip rate deduced for the last 5 My is a somewhat unreliable estimate because it is an average rate that integrates slip rate variation due to the tectonic regime changes (see below). Regardless, these estimates from plate kinematics and paleomagnetic studies do suggest a very high PKF slip rate of about 30–50 mm/yr. These rapid movements are confirmed by GPS data (e.g., Walpersdorf et al., 1998a,b), and by several uplifted coral terraces (Tjia and Zakaria, 1974; Beaudouin, 1998). The PKF lateral slip rate inferred from the 5 years' GPS measurements (1992–1996) is of 38 ± 6 mm/yr, as the most realistic far-field estimate (e.g. Vigny et al., 2002). In addition, using the U/Th series ages of the Donggala older uplifted marine terraces and ^{14}C ages of the younger ones (Beaudouin, 1998) the most realistic estimate yielded an uplift rate of about 1.8 mm/yr, that corresponds to a PKF left-lateral displacement velocity of about 30 ± 10 mm/yr for the present-day tectonic regime. Recent reappraisal of the long-term Holocene left-lateral slip rate for the PKF has been conducted by analysing the displacements of geomorphic features (Bellier et al., 2001). Horizontal, 370 ± 20 m, stream offsets incised within fans, whose surface abandonment has been dated at $11{,}000 \pm 2300$ yr using in situ-produced ^{10}Be cosmic ray exposure age (Bellier et al., 1999), yields a present-day lateral slip rate of 35 ± 8 mm/yr. These geologically determined long-term strike-slip rate agrees with the far-field velocity of 32–45 mm/yr deduced from GPS measurements.

6. Cooling and exhumation derived from fission track analysis, and Northern PKF rate deduced from vertical uplift

Structural analysis and morphological features provide evidence of uplift associated with the displacement of the northernmost segments of the PKF. However, in the Palu region, the fault system exhibits a significant component of dip-slip movement of which part is related to the releasing bend geometry and pull-apart development. The vertical component of the PKF motion has produced a 2300-m-high escarpment along the western edge of the Palu basin (Fig. 5A). According to the geology, the escarpment is of Late Miocene to Quaternary age. The escarpment is partly made up of

Table 1
Synthesis of geodynamic, geological, geomorphic and GPS data allowing to estimate PKF slip rates for different time span

Method	Features	Total displacement (m)	Age interval	Uplift rate (mm/yr)	Dip-slip rate (mm/yr)	Left-lateral slip rate (mm/yr)	Reference
Geodynamics	Plate kinematics	250. 10^3	5 Myr			50	Silver et al., 1983
Paleomagnetism	20° clockwise rotation of the SNA	150.10^3	5 Myr			30	Surmont et al., 1994
Geomorphic fan offset	Stream offset	280 to 420 ± 20	11+/−2.3 kyr			35 ± 8	Bellier et al., 2001
	Stream offset	370 ± 10	11+/−2.3 kyr			35 ± 15	Bellier et al., 2001
		3530 ± 20	125+/−20 kyr			29 ± 5	Bellier et al., 2001
	Coral terraces	10 to 210	Pleistocene to Holocene*	1.8	9 ± 2	30 ± 10	Beaudouin, 1998
Geological	Fault escarpment	2300	<7.7 Myr	>0.3 ± 0.01		>5,2 ± 2	This study
GPS	GPS measurements		1992–1996		3 ± 7	34 ± 3	Walpersdorf et al., 1998b
			1992–1999			38 ± 6	Vigny et al., 2002

SNA: Sulawesi northern arm; *ages of coral terraces are yielded by U–Th, ^{14}C and sea level correlation (see Beaudouin, 1998).

granodiorites related to the Younger Series defined by Elburg et al. (2003) of mafic-intermediate high-K magmas mainly emplaced in western Sulawesi from 14 and 5 Ma (K–Ar ages on biotite, Elburg et al., 2003), during a magmatic phase that occurred mainly prior to the collision of the Banggai–Sula block with the East arm at about 5 Ma (e.g., Hall, 2002). Sample 21*2 (Fig. 6) is within intrusive rocks related to the Tinombo Formation dated at about 40 Ma (44.1 ± 1.0; 44.8 ± 0.9; 37.5 ± 0.3; K–Ar ages on hornblende, Elburg et al., 2003). All the other samples (Fig. 6) are from the Younger Series (Elburg et al., 2003) while samples 22*1 and 22*2 are specifically from within the intrusive massif dated at 7.7 ± 0.2 Ma (K–Ar age on biotite, Elburg et al., 2003).

6.1. Fission-track analyses

Fission track-analysis was completed on granite and granodiorite samples collected along two sections (sample locations are presented on Fig. 6 and in Table 2, i.e., latitude, longitude, altitude). Due to the accessibility problem (high density forest cover), these sections are unfortunately discontinuous and the samples are scattered.

6.2. Analytical methods

Sample preparation followed the routine technique described by Seward (1989). Apatites were etched in 7% HNO_3 at 21 °C for 55 s and zircons in a eutectic mixture of KOH and NaOH at 210 °C for between 20 and 32 h. A mixture of 1HF:2HNO3:3HCl:6H2O (Naeser and McKee, 1970) was used for the titanites with an etch time of 20 min at room temperature. Irradiation was carried out at the ANSTO facility, Lucas Heights, Australia. Microscopic analysis was completed using an optical microscope with a computer driven stage ('Langstage' software from Dumitru, 1995). All ages were determined using the zeta approach (Hurford and Green, 1983) with a zeta value of 360 ± 5 for CN5/apatite, 432 ± 10 for CN5/titanite and 120 ± 5 for CN1/zircon (DS). They are reported as central ages (Galbraith and Laslett, 1993) with a 2 sigma error (Table 2). Where possible, 20 crystals of each sample were counted for age determination. The magnification used was ×1250 for apatite and titanite and ×1600 (oil) for zircon. Horizontal confined track lengths were measured at ×1250. In this study we assume an effective closure temperature for apatite of 110 ± 10 °C with a partial annealing zone from 110–60 °C (Green et al., 1989; Corrigan, 1993). The zircons can essentially be considered as having approximately zero alpha damage. This fact together with the calculated high cooling rate suggests that the appropriate closure is of the order of 300–320 °C (Rahn et al., 2004). For titanite the closure temperature is assumed to be 300 °C (Coyle and Wagner, 1998). Because of the very rapid cooling rates it is possible that all of these closure temperatures are too low but because of the extreme overlap in the different mineral ages at each site, this does not present a serious problem.

6.3. Results and interpretation

Nineteen fission-track ages are reported (Table 2), of which 9 were on apatite, 6 on zircon and 4 on titanite. All but one of these ages regardless of mineral phase, lie in the range 2.1 to 6.6 Ma. The only sample, that is drastically different (in age and lithology), is sample 21*2, which is situated to the north with an age (on apatite) of 18 ± 6 Ma. Because of the youthfulness of the samples very few track lengths in apatite could be measured, but those that were, yielded mean lengths in the range 14.4 to 15.5 μm (Table 2). At each site the different mineral ages overlap at 2 sigma error (Fig. 7A). The weighted means for zircon, titanite and apatite are 4.07 ± 0.39, 3.77 ± 0.29 and 3.27 ± 0.36 Ma, respectively (Fig. 7A).

The granodiorites and granites in this study belong to a group termed "Younger Series" by Elburg et al. (2003), with K–Ar biotite ages (closure temperature of about 350 °C, (McDougall and Harrison, 1988) ranging from 14–5 Ma (Fig. 7A). Samples 22*1 and 22*2 were from within the intrusive rock dated at 7.7 ± 0.2 Ma (Elburg et al., 2003). As in all geochronological methods, fission-track analysis also records the cooling of rocks through the respective closure temperatures of the minerals being analysed — in this case from ~310 to ~110 °C, (zircon to apatite). A possible break in slope in the cooling curve occurs at about 5 Ma at a time that the rocks had cooled to about 300 °C (Fig. 7A). This is followed by a very rapid cooling phase. The long track lengths in apatite (Table 2) indicate that this rapid cooling continued until the samples had passed through the lower temperature of the apatite partial annealing zone. This implies that rapid cooling lasted until at least a temperature of 60 °C was reached (break in slope on Fig. 7A). A very high cooling rate of 300 °C/my is estimated from ~4.1 to a little less than 3.3 Ma. From about 3.3 Ma, the cooling rate slowed down to about 12 °C/my. Exhumation rates estimated by examining the age–altitude relationships

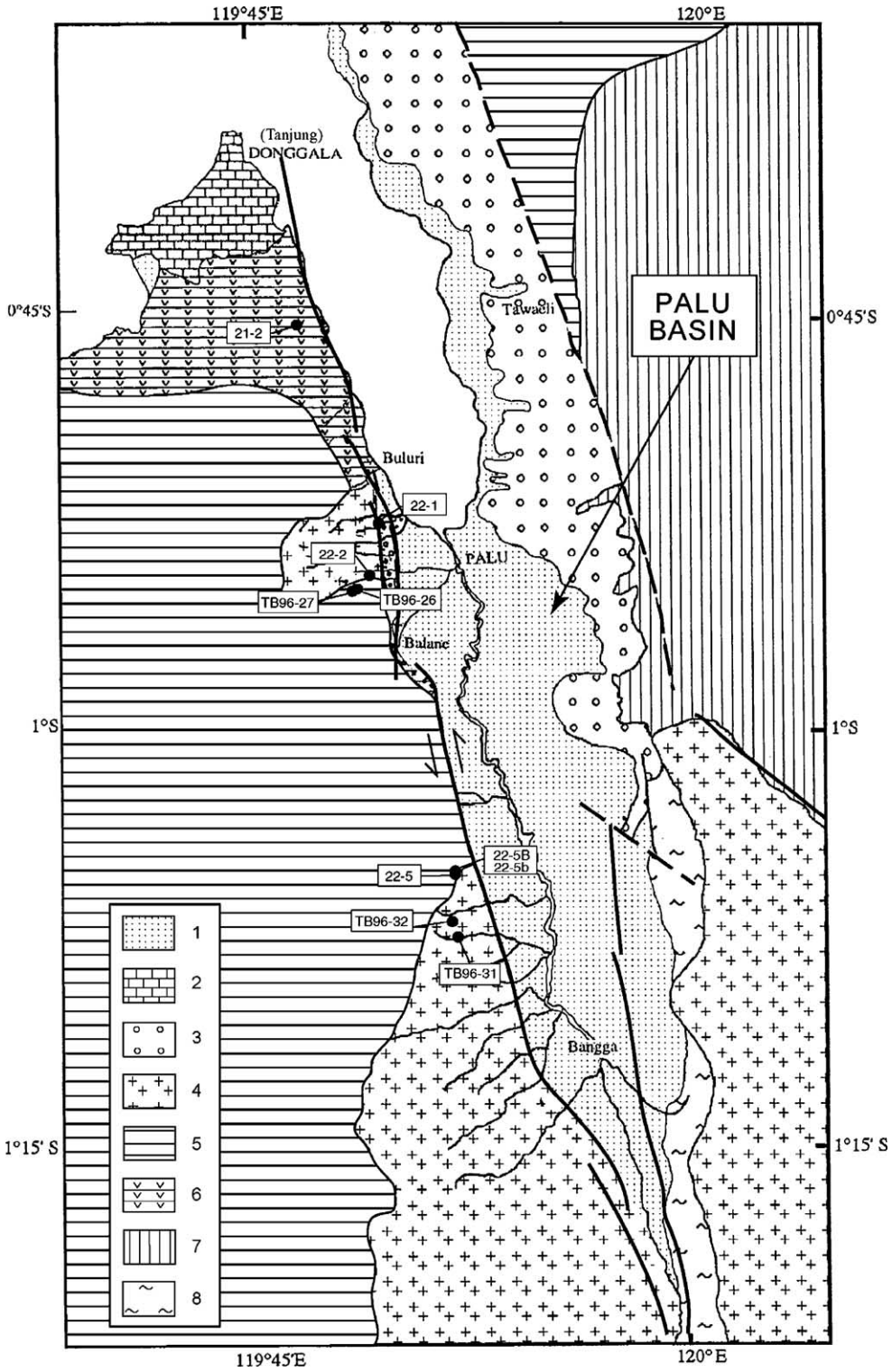

Fig. 6. Simplified geological map of the Palu domain (modified after Sukamto, 1973) where are reported the locations of fission-track samples (see the geographic coordinates in Table 2). 1 — Holocene alluvial deposits; 2 — Quaternary coral reef terraces; 3 — Mio-quaternary molasses, 4 — Mio-quaternary granitic rocks and granodiorites, 5 — Middle to Upper Eocene Tinombo Formation metamorphism, 6 — Tinombo Formation magmatism, 7 and 8 — metamorphic bedrock (7 — Cretaceous Latimonjong Formation; 8 — Triassic-Jurassic Gumbasa Formation).

Table 2
Fission-track ages from the western Palu Basin margin, Sulawesi

Sample number	Grid reference	Alt. (m)	Mineral	Irradiation number	Number of grains	Standard track density $\times 10^4$ cm^{-2} (counted)	$\rho_s \times 10^4$ cm^{-2} (counted)	$\rho_i \times 10^4$ cm^{-2} (counted)	$P(\chi^2)$ %	U (ppm)	Mean track length (μm)	Std dev (μm)	Age $\pm 2\sigma$ (Ma)
21*2	0°45′30″S 119°46′18″E	80	A	eth-92-6	18	141 (2451)	17.8 (119)	317 (2126)	0	28	14.49 ± 0.38 (6)	0.96	18 ± 6
22*1	0°52′36″S 119°49′10″E	220	Z	eth-109-9	20	44.0 (1374)	30.3 (333)	119 (1304)	0	30	–	–	6.58 ± 1.28
22*2	0°54′28″S 119°48′51″E	350	A	eth-92-13	20	126 (2451)	0.64 (8)	28.9 (360)	86	3	–	–	5.02 ± 3.6
TB 96*26	0°54′57″S 119°48′25″E	750	A	eth-92-12	20	128 (2451)	1.82 (19)	159 (1659)	28	16	–	–	2.64 ± 1.38
TB 96*26	°54′57″S 119°48′25″E	750	Z	eth-89-17	20	47.3 (2206)	39.0 (174)	221 (984)	94	182	–	–	5.01 ± 0.84
TB 96*27	0°55′02″S 119°51′51″E	930	A	eth-92-9	20	134 (2451)	2.75 (50)	150 (2732)	150	99	14 (1)	14.41	4.42 ± 1.28
22*5b	1°05′07″S 119°51′51″E	120	A	eth-92-7	14	139 (2451)	6.59 (46)	784 (5470)	73	70	14.38 ± 0.64 (4)	1.28	2.10 ± 0.62
22*5b	1°05′07″S S 119°51′51″E	120	Z	eth-89-19	12	45.9(2206)	120 (491)	693 (2835)	0	603	–	–	4.99±0.86
22*5b	1°05′07″S 119°51′51″E	120	T	eth-93-12	10	116 (3017)	31.2 (107)	2339(8034)	88	252	–	–	3.33 ± 0.66
22*5B	1°05′07″S 119°51′51″E	120	A	eth-92-14	20	123 (2451)	11.0 (98)	749 (6699)	93	76	15.05 ± 0.18 (15)	0.69	3.25 ± 0.66
22*5	1°05′10″S 119°51′51″E	150	A	eth-92-8	20	136 (2451)	11.0 (105)	813 (7738)	70	75	15.04 ± 0.59 (4)	1.18	3.33 ± 0.66
22*5	1°05′10″S S 119°51′51″E	150	Z	eth-89-23(2)	20	43.3 (2206)	126 (904)	972 (6988)	0.5	899	–	–	3.33 ± 0.36
22*5	1°05′10″S 119°51′51″E	150	T	eth-109-7	15	16.2 (756)	52.2 (424)	452 (3666)	5	350	–	–	3.95 ± 1.16
TB 96*31	1°07′25″S 119°51′57″E	220	A	eth-92-11	20	130 (2451)	8.5 (87)	506 (5182)	76	49	15.49 ± 0.46 (10)	0.80	3.92 ± 0.86
TB 96*31	1°07′25″S 119°51′57″E	220	Z	eth-89-18	20	46.6 (2206)	213 (570)	1476 (3944)	34	1267	–	–	4.05 ± 0.42
TB 96*31	1°07′25″S 119°51′57″E	220	T	eth-93-9	10	120 (3017	24.3 (77)	173 (546)	4	134	–	–	4.05 ± 1.10
TB 96*32	1°06′51″S 119°51′45″E	515	A	eth-92-10	20	132 (2451)	13.7 (87)	549 (3489)	49	52	15.02 ± 0.27 (10)	0.85	5.92 ± 1.30
TB 96*32	1°06′51″S 119°51′45″E	515	Z	eth-89-2	14	47.3 (2206)	240 (748)	1489 (4635)	0	1013	–	–	5.78 ± 0.98
TB 96*32	1°06′51″S 119°51′45″E	515	T	eth-109-6	9	16.15 (756)	24.3 (77)	173 (546)	99	0	–	–	4.72 ± 1.2

A = apatite, Z = zircon, T = titanite. ρ_s and ρ_i represent sample spontaneous and induced track densities; $P(\chi^2)$ is the probability of χ^2 for v degrees of freedom where v = no. of crystals − 1. All ages are central ages (Galbraith and Laslett, 1993). $\lambda_D = 1.55125 \times 10^{-10}$. Zeta = 360 ± 5 for apatite and CN5; 120 ± 5 for zircon and CN1; 432 ± 10 for titanite and CN5.

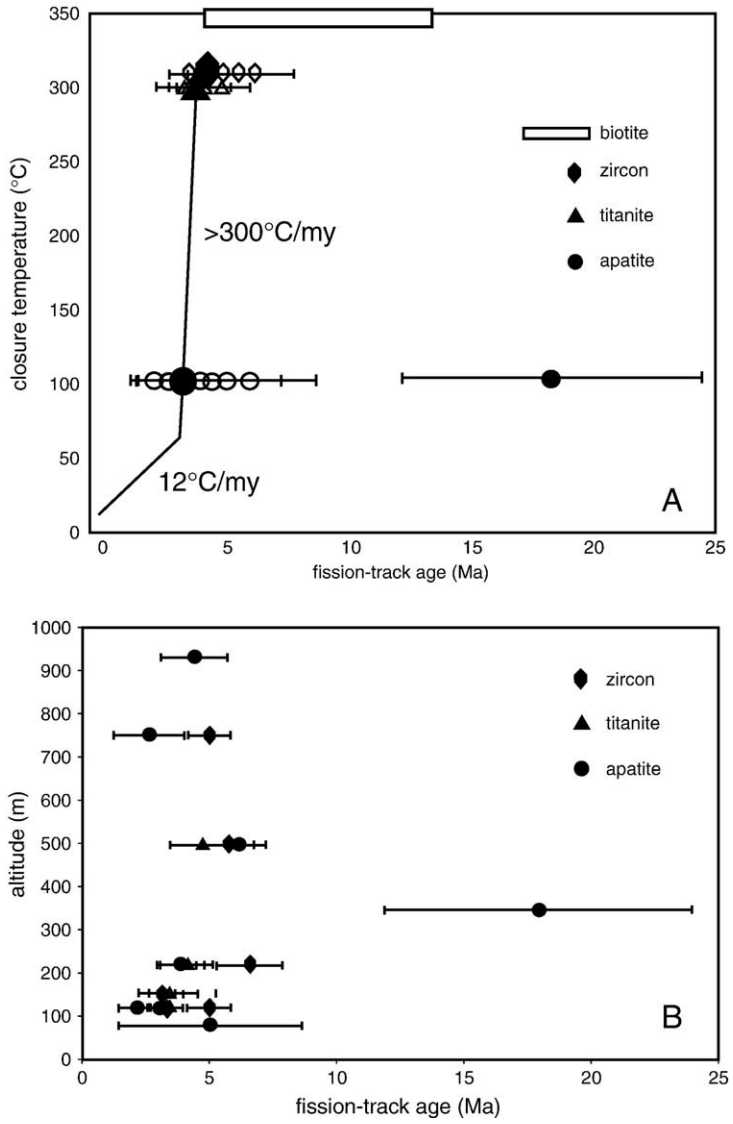

Fig. 7. Fission-track analysis results. 7A — Cooling history: K–Ar biotite ages from Elburg et al. (2003); 7B — age–altitude relationship.

(Fig. 7B) are of the order of 1 to 0.7 mm/y for the time period from 4.5 Ma to about 3 Ma.

As a second approach to estimating/confirming these exhumation rates, one may assume that the granites were intruded at a minimum depth of 3 km. Since the samples were taken from the base of a 2 km high granite escarpment, then at least 5 km has been eroded from above these sites. The age of the intrusion is >7.7 Ma (K–Ar biotite age, Elburg et al., 2003) — which leads to an absolute minimum denudation rate of 5 km in at least 7.7 Ma. That is, the minimum erosion rate was 0.65 mm/y. This is the equivalent of the minimum denudation rate estimated through the fission-track analysis.

6.4. Slip rate estimate from the escarpment analyses

The cumulative vertical displacement component (H) results from the uplift (h) and the subsidence component (Fig. 5b). The world-wide statistics (e.g., Van der Beek, 1996) as well as modelling (e.g., Hassani and Chéry, 1996) of tectonically active basins allow a relationship to be made between H and h such that $H=(5\pm1)*h$.

Striae on fault planes related to the present-day faulting measured along the PKF, provide slip-vector rakes ranging between 15° and 30°. Statistical analysis of slip-vector measured on the major PKF planes yields the most realistic mean rake (b) of about 15°

to 20° for present-day slip. In addition, measurement of the PKF major fault planes allows one to calculate a statistical mean fault dip ranging between 75° and 85°E that is in same order as the PKF 75 ± 12° dip, indirectly deduced from GPS measurements (Walpersdorf et al., 1998b).

From the uplift value, we can deduce the total vertical displacement (H), and knowing this vertical offset, the dip of the major fault plane (of about 80 ± 5°) and the present-day mean slip-vector (rake: 17.5±2.5°) on the plane, the horizontal component of the displacement (SS) can be calculated. The previously presented parameters imply the following relations: (1) SS=tg(90 − b) H/sinα, and for α=80 ± 5°, (2) SS=(3.3 ± 0,6)*H; where "α" is the fault dip; "b" the slip-vector pitch angle (rake); "SS" the strike-slip component; "H" the vertical displacement. The vertical component of the PKF motion has produced a 2300-m-high escarpment along the western edge of the Palu basin (Fig. 5a). Thus, from the minimum cumulative uplift that correspond to the escarpment high, we deduce the cumulative vertical displacement (H) ranges between 9200 and 13,800 m (Fig. 5b). Taking into account the value of 7.7 ± 0.2 Ma (Elburg et al., 2003), i.e. the age of the intrusive that formed the escarpment as being the maximum age of the escarpment genesis, an estimate of the minimum rock uplift rate has been calculated. It is of about 0.3 mm/yr (0.30 ± 0.01 mm/yr). Using the equations reported above, this corresponds to a PKF mean strike-slip rate (V_{ss}) 5.2 ± 2.0 mm/yr for about the last about 7.7 Ma, drastically lower than calculated from geomorphic feature offset for the Holocene (about 30–40 mm/yr, Bellier et al., 2001), i.e., for the present-day tectonic regime. However, both rock uplift rate and deduced left-lateral strike-slip fault velocity estimate, of about 0.3 and 3–7 mm/yr, respectively, are underestimated values because they take no account of erosion/exhumation, including a high rate of exhumation for the time period 4.5 – 3 Ma of the order of 0.7–1 mm/y calculated through our fission-track analyses. Nevertheless, for the recent time, in situ-produced ^{10}Be concentration analyses allows an estimate of average surficial erosion rates to be made. These are about ~6 m/Ma (0.006 mm/yr) in NW Sulawesi for the last 120 ka (Bellier et al., 1999), at least two orders of magnitude lower than the uplift rate estimated above. In fact, escarpment morphology with two distinct slope angles and a drastic slope change (triangular facet slope/above the facets) suggests that it is formed by several uplift stages and consequently by several phases of deformation (with different uplift/exhumation rate), as confirmed by the fault kinematics presented below.

7. Central Sulawesi fault kinematics

7.1. Methodology: inversion of fault slip data to determine the recent stress states

The kinematics of a fault population is defined using the striations measured on the fault planes at several sites. The sites of fault slip measurements are shown in Fig. 2, and the age of the faulted formations from which the striae were measured are given in the Table 3. We studied sites located on the 2 main faults, covering an area of approximately 100 × 100 km^2. The methodology of fault kinematic studies to determine paleostress fields and to demonstrate temporal and spatial changes in the late Cenozoic stress states has been used in many active tectonic areas around the world over past twenty years (e.g., see references in Mercier et al., 1991; Bellier and Zoback, 1995). To determine the stress fields responsible for recent deformation in the investigated area, we employed a quantitative inversion of distinct families of slip data determined at each individual site, using the method originally proposed by Carey (1979). These inversion results (see method in Table 3 captions) include the orientation (azimuth and plunge) of the principal stress axes (σ_1, $\sigma_2$and σ_3, correspond to the compressional, intermediate and extensional axes) of a stress tensor as well as a "stress ratio" $R=(\sigma_2-\sigma_3)/(\sigma_3-\sigma_1)$. Due to the out-crop conditions, strongly weathered and abundant vegetation cover, the measurement sites in Sulawesi are a meagre and data set is poorly distributed. However, several sites gave evidence of change in the paleo-kinematics. This study focuses on deformation from Late Miocene to Quaternary. Unfortunately, it is difficult to constrain the absolute age for fault striations more precisely than being younger than the age of the rocks cut by the faults. The striations analysed are observed along major fault planes affecting rocks of ages ranging between Tertiary and Quaternary. In general, more than one set of striae were detected at the same measurement locality. This may either be due to multiple slip within single events or to changes in slip directions driven by changes in the fault strength or boundary conditions. These distinct datasets can be geologically separated using structural arguments such as the relative striae cross-cutting relationships, i.e., relative chronology between striae, and their relation with regional tectonic events. We present significant fault kinematic datasets that provide evidence for the recent tectonic regime

Table 3
Results of stress tensor inversion for slip data representing Late Cenozoic faulting stress regimes

SITE	N	σ_1		σ_2		σ_3		R	Relative chronology	Age	Site locations
		Azim.	Dip	Azim.	Dip	Azim.	Dip				
Donggala		WNW–ESE				NNE–SSW				Quaternary	0°39,25′S 119°44,30′E
tanjung				NNW–ESE		NNE–SSW					
				N–S		E–W					
Pangga	16	186	6	94	21	290	68	0.5	1	Eocene–Oligocene	0°43,25′S 119°46,50′E
	6	6	65	179	25	270	3	0.05	2	Tinombo	
Lekatu and		NW–SE				NE–SW			1	Eocene Tinombo	0°51,42′S 119°48,65′E
buluri				N–S		E–W			2		
		WNW–ESE				NE–SSW			3		
Balaroa				NW–SE		NE–SW			1	Late Tertiary	1°01,50′S 119°51,40′E
		WNW–ESE				NNE–SSW			2	metamorphic	
Kawua	7	155	11	246	7	8	77	0.99	1	Late Tertiary	1°24,50′S 120°45,40′E
	9	336	87	95	2	186	3	0.82	2 or 3		
	5	328	87	95	2	185	3	0.82	2 or 3		
	17	308	58	132	32	41	1	0.11	2 or 3		
Saluopa	10	118	0	208	39	27	51	0.75	1	Lower Tertiary	1°47,00′S 120°32,10′E
	10	117	0	222	90	27	0	0.92	1		
					NNE–SSW				2		
Wuko				N–S		E–W			1	Quaternary	1°46,40′S 120°32,80′E
				WNW–ESE		NNE–SSW			2		
Kolahi		WNW–ESE							1	Cretaceous to	2°01,50′S 120°37,00′E
						NNE–SSW			2	Paleocene	
Bancea		E–W		N–S					1	Cretaceous to	1°59,45′S 120°35,00′E
				E–W		N–S			2	Paleocene	

Table 3B

Combined population sites	N	σ_1		σ_2		σ_3		R	Relative chronology	Age
		Azim.	Dip	Azim.	Dip	Azim.	Dip			
Saluopa kolahi and kawua	21	122	3	32	10	230	79	0.88	1	Tertiary
Bancea and kawua	8	96	4	186	7	332	82	0.5	1b	Cretaceous to Tertiary
Saluopa and wuko kolahi and kawua	23	34	83	277	3	187	6	0.65	3	Tertiary to Quaternary
Wuko and kawua	8	174	72	347	18	78	2	0.51	2	Late Tertiary to Quaternary

The used inversion method (e.g., Carey, 1979) assumes that the slip represented by the striation (s) occurs in the direction of the resolved shear stress (τ) on each fault plane, the fault plane being a pre-existing fracture. Inversion computes a mean best-fitting deviatoric stress tensor from a set of striated faults by minimising the angular deviation between a predicted slip-vector (maximum shear, τ) and the observed striation (s). The results of the stress inversion are generally considered reliable if 80% of the deviation angles (angle between the calculated slip-vector "τ" and the striation "s") are less than 20°. For robust datasets (including a wide variety of slip vectors and fault plane orientations) these methodologies yield similar results (Mercier et al., 1991). In the Site column, "&" indicates an inversion solution computed from two or more datasets from different sites, for example Lacato & Buluri corresponds to an inversion computed from dataset of sites Lacato and Buluri. In Table 3B are inversion results 18/08/05 31 from several site combined dataset. N=number of striated fault planes used to compute the solutions. Deviatoric principal stress axes: σ_1, σ_2, σ_3, are the compressional, intermediate and extensional deviatoric axes, respectively. $R=(\sigma_2-\sigma_1)/(\sigma_3-\sigma_1)$, is the "stress ratio" of the deviatoric stress tensor, a linear quantity describing relative stress magnitudes. Relative chronology of the fault kinematics is based on striae crosscutting relationships. Ages are reported from the geological map (GRDC) and Van Leeuwen and Muhardjo (2005).

change and we report in Table 3 the relative chronology that results from the superimposed slip-vectors measured at several sites. Particularly for striae affecting Tertiary rocks, the crosscutting relationships on fault planes indicate a succession of faulting phases. These crosscutting relationships between striations allowed the determination of the Late Miocene to present-day stress histories that corresponds to three distinct regional tectonic regimes.

7.2. Palu–Koro Fault kinematics

The present-day transtensional tectonic regime suggested from the geomorphic survey has been confirmed by the fault kinematic analyses, i.e. by the slip-vector measurements on fault planes. Indeed, we constrained Late Cenozoic stress regimes within the NNW-trending PKF using inversions of slip-vectors measured on both major and minor faults. Slip chronologies measured on

several independent fault planes show striations that indicate oblique (left-lateral) reverse faulting cross-cut by normal slip striations on the same fault planes. These normal slip striations are affected themselves, by normal component left-lateral strike-slip striations. These different families of cross-cutting striae shown by angular deviations (rake) of $30 \pm 10^{\circ}$ have been detected at several sites along the PKF. Because the successions are similar at the different sites, it is assumed that they indicate changes in the Late Cenozoic stress regime (magnitudes and/or orientation) rather than multiple slip. Consequently, these data indicate significant variations during Late Cenozoic time both in principal stress orientations and relative magnitudes as reflected by faulting ranging from oblique reverse-slip, oblique- to pure normal-slip, and strike-slip which reactivated inherited Tertiary structures and/or produced new faults. Examples of lower hemisphere stereoplots of inversion results from three distinct slip orientations on the PKF System are reported in Fig. 8 (kinematics sites are synthesised in the Table 3). They indicate:

(1) An oblique left-lateral reverse movement associated with pervasive deformations that correspond to a transpressional stress regime characterised by NW- to NNW-trending σ_1 axis. However, at the Pangga site slip-vector analyses of minor faults, affecting the Eocene–Oligocene Tinombo Formation (age from Van Leeuwen and Muhardjo, 2005), provide evidence for a compression with a N186°E-trending σ_1 axis. It could correspond to a post-Oligocene stress regime in the Late Cenozoic collision history of Sulawesi and/or to a heterogeneity of the deformation within the transpressional stress regime described above.
(2) Normal faulting related to an E-trending extension.
(3) The recent left-lateral strike-slip faulting with a slight normal component, characterised by striations on calcite-fault-rocks and gouge, corresponding to transtensional regime with a N to NE-trending σ_3 axis. The focal mechanism from the January 2005 (M_w-6.2) earthquake recorded around the northern offshore PKF is consistent with a left-lateral strike-slip combined with normal faulting, showing that the transtensional regime corresponds to the present-day activity.

Nevertheless, in the Donggala region (Tangjung and Donggala sites), measurements in Quaternary coral reef formations provide evidence for a recent heterogeneous (majority dip-slip, e.g. Beaudouin, 1998) normal faulting that we interpret as recent gravitational effects, subsequent to the present-day transtensional stress regime. However, the major penetrative striae are indicating a recent (syn- to post-Pleistocene) left-lateral with a small normal component displacement (see stereonet "Tanjung maj." in Fig. 8).

In conclusion, the recent and present-day fault kinematics are characterised by left-lateral movement with a slight normal component (stereonet, Fig. 8). However, three main regional phases of deformation have been identified, from oldest to youngest they are: 1) a transpressional (strike-slip to oblique reverse-slip) stress regime characterised by NW-trending σ_1 axis; 2) a collapse effect normal faulting stress regime characterised by about W-trending σ_3 axis, and 3) a recent and present-day transtensional strike-slip regime with about WNW-trending σ_1 and NNE-trending σ_3 axes, confirmed by geomorphic observations and geodetic measurements as described previously.

7.3. Poso domain fault kinematics

Similarly in the Poso domain we provide evidence for a homogeneous succession of fault kinematics from minor and major faulting in formations from Cretaceous to Quaternary at the different sites. Faulting in Tertiary and Quaternary formations provides evidence for changes in the Late Cenozoic stress regime. Thus, this data indicate significant stress variations during the Late Cenozoic as testified by faulting ranging from oblique reverse-slip, oblique-to pure normal-slip.

Fault measurement sites are reported in Table 3, while inversions of combined data sets are presented in Table 3B. Lower hemisphere stereoplots of inversion results from three distinct slip orientations from the Poso region are reported in Fig. 9. These fault slip-vector analyses show a succession of 3 major tectonic regimes. The first corresponds to reverse faulting consistent with a compressional stress regime characterised by a WNW-trending compression. It could be divided into two subsequent stress regimes: a first with a N96°E- trending and a second with a N122°E-trending σ_1 axes, respectively. The second regional stress regime is represented by normal slip striae and corresponds to an E-trending extension. The last one testifying to the Recent to present-day regime is marked by faint normal faulting striations measured on fault planes affecting Quaternary deposits. This corresponds to extensional tectonics characterised by N174°E-trending σ_3 axis, closely parallel to the σ_3 axis evidence for the present-day transtensional regime acting along the PKF.

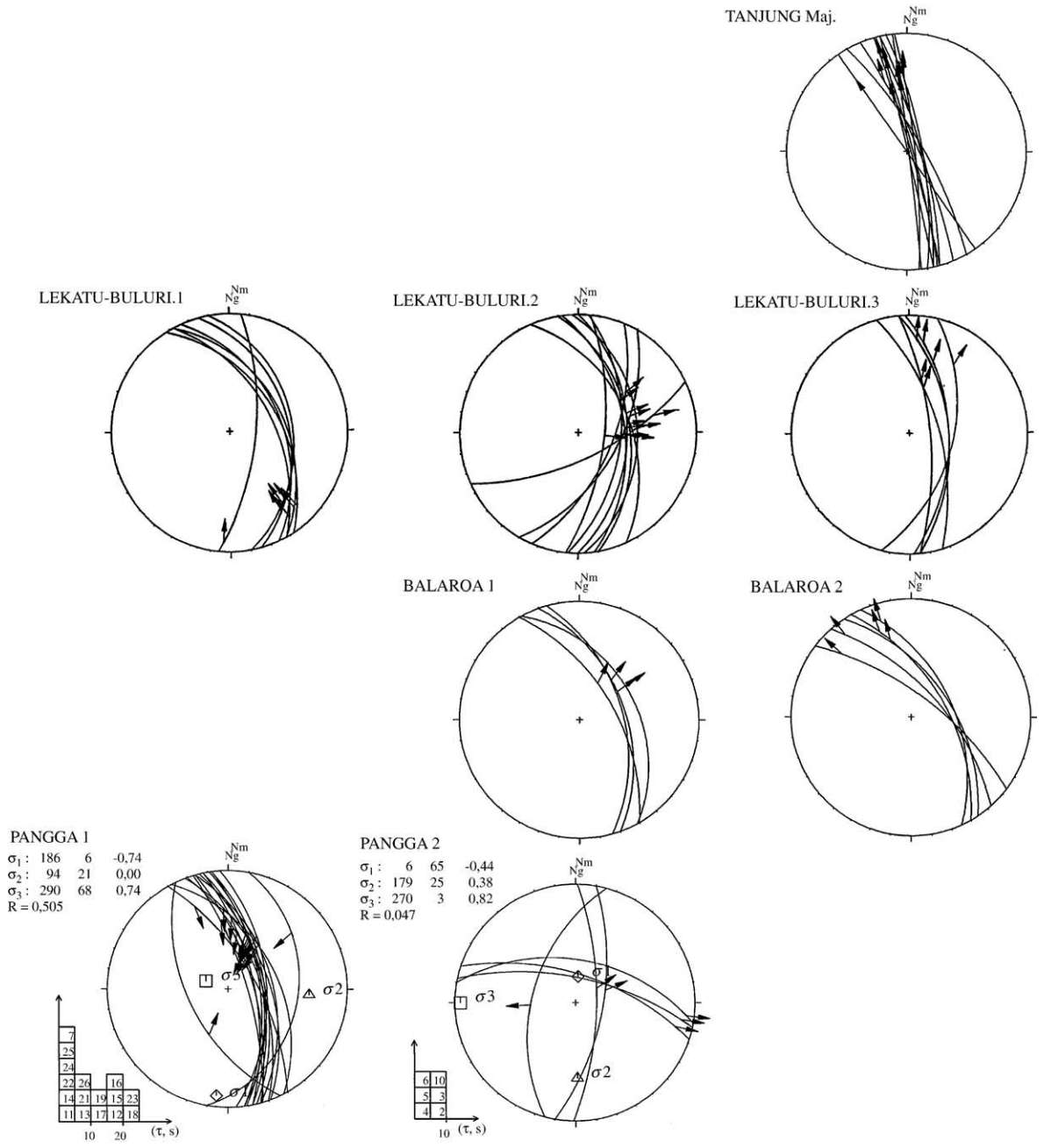

Fig. 8. Examples of lower hemisphere stereoplots of respectively reverse-strike-slip faulting, normal-slip faulting and normal-strike-slip faulting data from Palu–Koro fault region. Labels outside and to the right of the stereonets refer to sites located on Fig. 2, and reported in Table 3. Pangga 1 and Pangga 2 stereonets presents fault kinematics together with results determined by Carey's (1979) inversion method, presented in Table 3. The results include deviatoric stress parameters (σ_1, σ_2 and σ_3 axes) determined by Carey's (1979) inversion method, i.e., azimuth, plunge and relative magnitudes of the principal axes as well as the stress ratio value ($R = \sigma_2 - \sigma_1 / \sigma_3 - \sigma_1$).

7.4. Discussion and conclusion

In the current study we present a tectonic analysis of the CSFS that is a fault system comprising left-lateral strike-slip fault zones, where shallow earthquake activity is documented. We define, from west to east, the occurrence of two major active fault systems: the NNW-trending PKF and the southeast Sulawesi distributed fault system (Figs. 1 and 2). Even though deformation is distributed over three fault zones in the east-

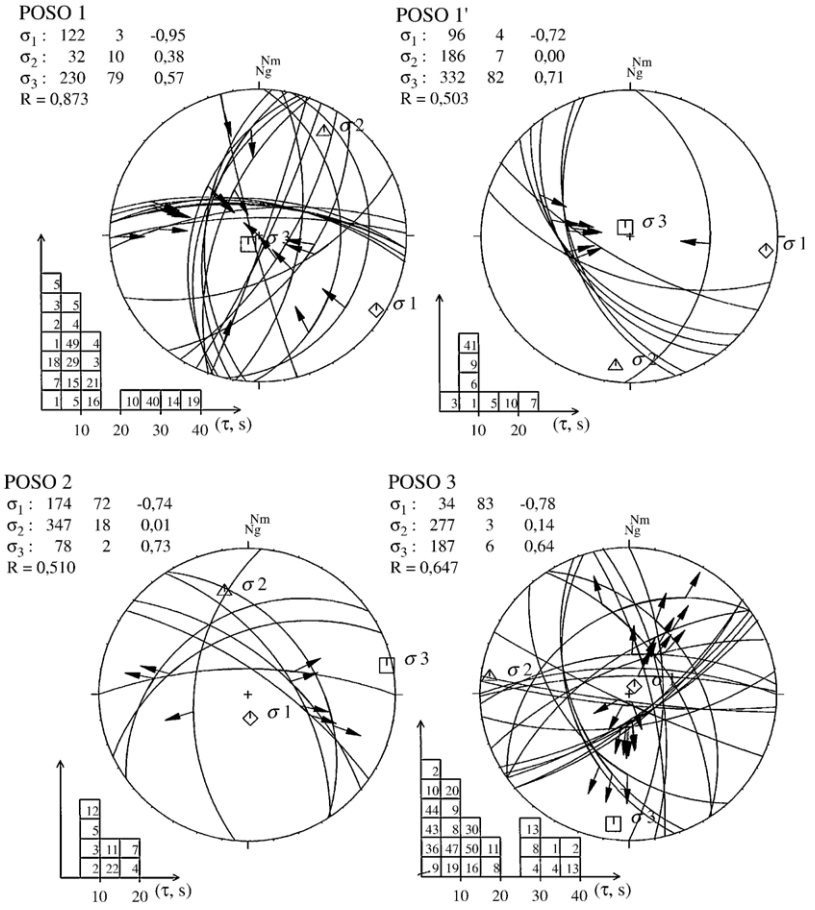

Fig. 9. Lower hemisphere stereoplots of successive faulting for the Poso region. Same caption as in Fig. 8. Poso 1 represents combined fault population and inversion result from sites of Saluopa, Kolahi and Kawua; Poso 1' of Bancea and Kawua; Poso 2 of Wuko and Kawua; Poso 3 of Saluopa, Wuko, Kolahi and Kawua (see Table 3, and location in Fig. 2).

central part and SE arm of Sulawesi, the majority of the active deformation occurred on the W to WNW-trending Matano Fault. Several arguments provide evidence for a northward migration of the fault activity in the SE arm to the eastern central Sulawesi from the Mendoke, to the Lawanopo then the Matano Fault (Beaudouin, 1998). This migration probably results from the accommodation of the successive collisions during the Late Cenozoic and the consequent block rotations.

Study of the PKF segments provides evidence for Late Quaternary geomorphic features associated with strike-slip faulting; these include streams displaced by left-lateral faults, alluvial fan offsets and shutter ridges. The western edge of the Palu basin is controlled by a N to NNW-trending 2300 m high escarpment of which the foot is marked by facetted spurs and at about 300 m high triangular and trapezoidal facets. The significant normal slip component of the present-day faulting, suggested by the faceted escarpment, is confirmed by a succession of Quaternary uplifted coral reefs, of which the highest reaches 210 m in height, along the coast at the east of the Palu Gulf, in NW Sulawesi (Donggala area Fig. 6, e.g., Beaudouin, 1998). These combined geomorphic characteristics evidence coeval strike-slip and normal faulting for the present-day northern PKF activity, that corresponds to a transtensional tectonic regime confirmed by the analyses of the fault kinematics, i.e. by the slip-vector measurements on fault planes. The focal mechanism from a recent M_w=6.2 earthquake that occurred in January 2005 is consistent with this transtensional stress regime, suggesting that this regime is currently active.

An along-strike survey of the Sulawesi faults was performed, analysing and dating fault offsets for the purpose of estimating the long-term slip-rate on the fault. Left-lateral displacement of 370 ± 10 m of streams incised within fans (Bellier et al., 2001), whose deposition has been dated at $11{,}000 \pm 2300$ yr, (Bellier et al., 1999), yields a calculated PKF horizontal slip rate of 35 ± 8 mm/a. This geologically determined

long-term slip rate agrees with the far-field strike-slip rate of 32–45 mm/a previously proposed from GPS measurements (e.g., Vigny et al., 2002) and confirms that the PKF is a fast slipping fault with a relatively low level of seismicity (e.g., Bellier et al., 1998, 2001).

A previous study (Bergman et al., 1996) reported results from a fission-track study applied further south along the western domain of Sulawesi suggested a rapid regional cooling event between 5 and 6 Ma. The current fission-track analyses of the granodiorites at the western edge of the Palu basin also document a major rapid cooling period but between about 4.1 and 3 Ma.

Combined geomorphic, fission-track and fault kinematics analyses of the PKF escarpment bounding the Palu basin argue for a complex escarpment morphogenesis history and help to constrain the vertical slip rate (including uplift/erosion rates). Fission-track analysis provide evidence for a rapid cooling between about 4.1 and 3.3 Ma. Examining the fission-track ages versus altitude relationships of magmatic rocks that form the escarpment of Palu basin western edge, we calculated estimates for the exhumation rate of the order of 0.7–1 mm/yr during the Pliocene (for a time period ranged between about 4.1 and 3 Ma).

The reason for the increase in cooling rates could either be due to re-adjustment of the geotherms after a period of magmatic activity or to an increase in erosion rates or both. However, recent geological studies have revealed that large volumes of coarse material were being deposited to the west from the beginning of the Pliocene (Calvert, 2000; Calvert and Hall, 2003). This hence supports the notion that rapid exhumation of the source regions began at about this time and is directly correlative with the timing estimated from the fission-track data sets. Thus, the cooling seen through the fission-track analysis is most likely to be related to a phase of increased erosion.

This increase probably results from combined effects of both: 1 — the rapid regional uplift and associated erosion already mentioned by Bergman et al. (1996) between 5 and 6 Ma, as a result of the collision between the Banggai–Sula block and East Sulawesi that induces in NW Sulawesi a transpressional regime; 2 — local uplift of the shoulder of the western edge of the Palu basin due to a collapse normal faulting during the Pliocene (see fault kinematics study).

Fault kinematic analysis documents changes in the tectonic regime since about the Miocene. The older Late Cenozoic fault kinematics (probably Late Miocene–Pliocene in age, i.e., coeval to the last collision that occurred at about 5 Ma) shown along the PKF corresponds to a transpressional (left-lateral kinematics with a reverse component) tectonic regime with a WNW- to NW-trending σ_1. It is represented by pervasive deformation that corresponds within the Poso domain with a reverse faulting stress regime with a WNW-trending σ_1. This event is probably coeval with the collision between the Banggai–Sula blocks and East Sulawesi of which the climax occurred in Pliocene (about 5 Ma, e.g., Hall, 2002). In the Palu region, the collision produced a transpressional (oblique-strike-slip displacement with a reverse component) stress regime because the PKF zone accommodates two combined effects resulting from the collision, a direct shortening–thickening effect of the collision, and the northward extrusion of the Central Sulawesi block, i.e. clockwise rotation driven by the PKF, consequent to the collision.

Subsequently, a collapse effect seen in a normal faulting stress regime is characterised by about W-trending σ_3 axis. It is regionally observed within the Palu to Poso domains. Part of the rapid uplift that we report, could be related to the Palu basin edge uplift related with normal faulting consequent from collapse and exhumation processes.

Recent geological studies, and a reappraisal of the stratigraphy of West Sulawesi (Calvert, 2000; Calvert and Hall, 2003) support the notion that rapid exhumation began at about 5 Ma. Granites were being intruded between 14 and 5 Ma, and there is no evidence for large amounts of erosion related to unroofing before the Pliocene. Based on the stratigraphy, one might expect slow cooling immediately after intrusion until about 5 Ma and then more rapid cooling associated with the exhumation. The major cooling event seen through the fission-track data at 4.1–3. Ma can be related to exhumation as evidenced from large volumes of coarse material reported by Calvert and Hall (2003) that were being deposited at this time to the west.

Finally a transtensional regime followed. It characterises the present-day kinematics that continue to "drive" the Central Sulawesi block's northward extrusion and clockwise rotation along the PKF. It corresponds to a NNE-trending extensional regime in the Poso domain up to the Tomini Gulf. Indeed, focal mechanisms within the southern zone of the Tomini Gulf (Beaudouin et al., 2003) testify of an extensional stress regime with a NE-trending σ_3. Taking into account the position of the Tomini Gulf and of the Poso zone, this deformation could be interpreted as a back-arc spreading effect due to the activity of the North Sulawesi subduction. This spreading producing extensional internal deformation within the Central Sulawesi

block in agreement with the suggestions of Central Sulawesi block normal faulting deduced from GPS measurements (Walpersdorf et al., 1998a) and earthquake focal mechanisms determined from a microseismicity survey (McCaffrey and Sutardjo, 1982). In addition, unpublished offshore seismic data (industry) show that there has been intermittent west-propagating thrusting since the beginning of the Pliocene, and this irregular advancement of thrusting could also cause the changes from transpressional, to extensional, to transtensional deformations within Central Sulawesi (R. Hall, personal communication).

Acknowledgements

This study was developed in the framework of an ASEAN-EU project, the "GEODYSSEA project," a portion of the programme was set apart for studying the tectonics and active faulting in Sulawesi. The Sulawesi project complemented the joint proposal for an extensive GPS project submitted to the EC and ASEAN entitled "Plate motions and crustal deformations deduced from space geodetic measurements for the assessment of related natural hazards in South East Asia". We thank both P3G and DGGMR for field work assistance. Funding was provided by the E.U. through the "GEODYSSEA" project and the PICS "Indonésie" (INSU-CNRS). SPOT images were provided thanks to the ISIS programme support (CNES). We thank M. Polvé, R. Maury and M. Elburg for providing information about the "Younger series" and Th. M. Van Leeuven for providing an unpublished manuscript. Special thanks are due to Jean-Jacques Cochemé that analysed with us, thin-sections of the studied magmatic rocks, and to Geneviève Roche (UMR OrsayTerre, UP Sud) and Jean-François Brouillet (UMR-Tectonique, Paris) for drawing several figures of this paper. R. Hall and an anonymous reviewer are thanked for their reviews which greatly improved the manuscript.

References

Beaudouin, T., 1998. Tectonique active et sismotectonique du système de failles décrochantes de Sulawesi Central. Ph-D Thesis, Univ. Paris-Sud. 343 pp.

Beaudouin, Th., Bellier, O., Sébrier, M., 2003. Champs de contrainte et de déformation actuels de la région de Sulawesi (Indonésie): implications géodynamiques. Bull. Soc. Géol. Fr. 174, 305–317.

Bellier, O., Beaudouin, Th., Sébrier, M., Villeneuve, M., Bahar, I., Putranto, E., Pratomo, I., Massault, M., Seward, D., 1998. Active faulting in Central Sulawesi (Eastern Indonesia). In: Wilson, P., Michel, G.W. (Eds.), The GEODYnamics of S and SE Asia (GEODYSSEA) Project Final Report, EC contract CI1*CT93-0337, Scient. Technical Rep. STR, vol. 98-14, pp. 276–312.

Bellier, O., Zoback, M.L., 1995. Recent state of stress change in the Walker Lane zone, Western Basin and Range — USA. Tectonics 14, 564–593.

Bellier, O., Bourles, D., Beaudouin, M., Braucher, R., 1999. Cosmic Ray Exposure (CRE) dating in wet tropical domain: late Quaternary fan emplacements in central Sulawesi (Indonesia). Terra Nova 11, 174–180.

Bellier, O., Sébrier, M., Beaudouin, Th., Villeneuve, M., Braucher, R., Bourles, D., Siame, L., Putranto, E., Pratomo, I., 2001. High slip rate for a low seismicity along the Palu–Koro active fault in central Sulawesi (Indonesia). Terra Nova 13, 463–470.

Bergman, S.C., Coffield, D.Q., Talbot, J.P., Garrard, R.A., 1996. Tertiary Tectonic and magmatic evolution of western Sulawesi and the Makassar Strait, Indonesia: evidence for a Miocene continent–continent collision. In: Hall, R., Blundell, D. (Eds.), Tectonic Evolution of Southeast Asia, Geol. Soc. Spec. Publ. Lond., vol. 106, pp. 391–429.

Calvert, S.J., 2000. The Cenozoic evolution of the Lariang and Karama basins, Sulawesi. 27th Annual Convention, Jakarta, Indonesian Petroleum Association, Proceedings, pp. 505–511.

Calvert, S.J., Hall, R., 2003. The Cenozoic geology of the Lariang and Karama regions, western Sulawesi: new insight into the evolution of the Makassar straits region. 29th Annual Convention, Jakarta, Indonesian Petroleum Association Proceedings, IPA03- G-036, pp. 501–517.

Carey, E., 1979. Recherche des directions principales de contraintes associées au jeu d'une population de failles. Rev. Géol. Dyn. Géogr. Phys. 21, 57–66.

CMT, Harvard University Moment Tensor catalog (CMT Project), 2005. Online Data Set: http://www.seismology.harvard.edu/projects/CMT/CMTsearch.html.

Corrigan, J.D., 1993. Apatite fission-track analysis of Oligocene strata in South Texas, U.S.A. testing annealing models. Chem. Geol. 104, 227–249.

Coyle, D.A., Wagner, G.A., 1998. Positioning the titanite fision-track partial annealing zone. Chem. Geol. 149, 117–125.

Daly, M.C., Cooper, M.A., Wilson, I., Smith, D.G., Hooper, B.G.D., 1991. Cenozoic plate tectonics and basin evolution in Indonesia. Mar. Pet. Geol. 8, 2–21.

Dumitru, T.A., 1995. A new computer automated microscope stage system for fission track analysis. Nucl. Tracks Radiat. Meas. 21, 575–580.

Elburg, M., van Leeuwen, Th., Folden, J., Muhardjo, 2003. Spatial and temporal domains of contrasting igneaous suites in Western and Northern Sulawesi, Indonesia. Chem. Geol. 199, 243–276.

Galbraith, R.F., Laslett, G.M., 1993. Statistical models for mixed fission-track ages. Nucl. Tracks Radiat. Meas. 21, 459–470.

Green, P.F., Duddy, I.R., Laslett, G.M., Hegarty, K.A., Gleadow, A.J.W., Lovering, J.F., 1989. Thermal annealing of fission tracks in apatite: 4. Quantitative modelage techniques and extension to geological time scales. Chem. Geol. 79, 155–182.

G.R.D.C., Geological Research and Development Centre, 1981-1993. Geological map of Sulawesi, scale 1/250.000. G.R.D.C. Press, Bandung.

Hall, R., 1996. Reconstructing Cenozoic SE Asia. In: Hall, R., Blundell, D. (Eds.), Tectonic Evolution of Southeast Asia, Geol. Soc. Spec. Publ. Lond., vol. 106, pp. 153–184.

Hall, R., 2002. Cenozoic geological and plate tectonic evolution of SE Asia and SW Pacific: computer-based reconstructions, model, and animation. J. Asian Earth Sci. 20, 353–431.

Hall, R., Wilson, M.E.J., 2000. Neogene sutures in eastern Indonesia. J. Asian Earth Sci. 18, 781–808.

Hamblin, W.K., 1976. Pattern of displacement along the Wasatch fault. Geology 4, 619–622.
Hamilton, W., 1979. Tectonics of the Indonesian region. U. S. Geol. Surv. Prof. Pap. 1078. 345 pp.
Hassani, R., Chéry, J., 1996. Anelasticity explains topography associated with basin and range normal faulting. Geology 24, 1095–1098.
Hinschberger, F., Malod, J.A., Rehault, J.P., Dyment, J., Honthaas, C., Villeneuve, M., Burhanuddin, S., 2000. Origine et évolution du bassin Nord-Banda (Indonésie): apport des données magnétiques. C. R. Acad. Sci. (Paris) 331, 507–514.
Hurford, A.J., Green, P.F., 1983. The zeta age calibration of fission-track dating. Chem. Geol. 41, 285–317.
Katili, J.A., 1970. Large transcurrent faults in Southeast Asia with special reference of Indonesia. Geol. Rundsch. 59, 581–600.
Katili, J.A., 1975. Volcanism and plate tectonics in the Indonesian Island Arcs. Tectonophysics 26.
McCaffrey, R., Sutardjo, R., 1982. Reconnaissance microearthquake survey of Sulawesi, Indonesia. Geophys. Res. Lett. 9, 793–796.
McDougall, I., Harrison, T.M., 1988. Geochronology and thermochronology by $^{40}Ar/^{39}Ar$ method. Oxford Press, Oxford, UK. 212 pp.
Mercier, J.L., Carey-Gailhardis, E., Sébrier, M., 1991. Paleostress determinations from fault kinematics: application to the neotectonics of the Himalayas–Tibet and the Central Andes. Philos. Trans. R. Soc. Lond., A 337, 41–52.
Naeser, C.W., McKee, E.H., 1970. Fission-track and K–Ar ages of Tertiary ash-flow tuff, north-central Nevada. Geol. Soc. Am. Bull. 81, 11, 3375–3384.
Polvé, M., Maury, R.C., Bellon, H., Rangin, C., Priadi, B., Yuwono, S., Joron, J.L., Soeria Atmadja, R., 1997. Magmatic evolution of Sulawesi (Indonésia): constraints on the Cenozoic geodynamic history of the Sundaland active margin. Tectonophysics 272, 69–92.
Polvé, M., Maury, R.C., Vidal, Ph., Priadi, B., Bellon, H., Soeria Atmadja, R., Joron, J.L., Cotten, J., 2001. Melting of lower continental crust in a young post-collision setting: a geochemical study of Plio-Quaternary acidic magmatism from central Sulawesi (Indonesia). Bull. Soc. Géol. Fr. 174, 305–317.
Rahn, M.K., Brandon, M.T., Batt, G.E., Garver, J.I., 2004. A zero-damage model for fission-track annealing in zircon. Am. J. Sci. 89, 473–484.
Rangin, C., 1989. The Sulu Sea, a back-arc basin setting within a Neogene collision zone. Tectonophysics 161, 119–141.
Seward, D., 1989. Cenozoic basin histories determined by fission track dating of basement granites, South Island, New Zealand. Chem. Geol. 79, 31–48.
Silver, E.A., McCaffrey, R., Smith, R.B., 1983. Collision, rotation, and the initiation of subduction in the evolution of Sulawesi, Indonesia. J. Geophys. Res. 88, 9407–9418.
Stevens, C., McCaffrey, R., Bock, Y., Genrich, J., Endang, Subarya, C., Puntodewo, S.S.O., Fauzi, Vigny, C., 1999. Rapid rotations about a vertical axis in a collisional setting revealed by the Palu fault, Sulawesi, Indonesia. Geophys. Res. Lett. 26, 2677–2680.
Sukamto, R., 1973. Reconnaissance geological map of Palu area, Sulawesi. Geological map, scale 1 :250.000. Geological Survey of Indonesia, Bandung, Indonesia.
Surmont, J., Laj, C., Kissel, C., Rangin, C., Bellon, H., Priadi, B., 1994. New paleomagnetic constraints on the Cenozoic tectonic evolution of the North arm of Sulawesi, Indonesia. Earth Planet. Sci. Lett. 121, 629–638.
Tjia, H.D., 1981. Example of young tectonism in Eastern Indonesia. In: Barber, A.J., Wiryosudjono, S. (Eds.), The Geology and tectonics of Eastern Indonesia, Spec. Publ Geol. Res. and Dev. Centre, Bandung, Indonesia, vol. 2, pp. 89–104.
Tjia, H.D., Zakaria, T.H., 1974. Palu–Koro strike slip fault Zone, Central Sulawesi, Indonesia. Sains Malays. 3, 67–88.
Van der Beek, P.A., 1996. Tectonic evolution of continental rifts: inférences from numerical modelling and fission track thermochronology. Proefschrift Vrije Universiteit, Amsterdam. 232 pp.
Van Leeuwen, Th., Muhardjo, M., 2005. Stratigraphy and tectonic setting of the Cretaceous and Paleogene vocanic-sedimentary successions in northwest Sulawesi, Indonesia: implication for the Cenozoic evolution of Western and Northern Sulawesi. J. Asian Earth Sci. 25, 481–511.
Vigny, C., Perfettini, H., Walpersdorf, A., Lemoine, A., Simons, W., Van Looon, D., Ambrosius, B., Stevens, C., McCaffrey, R., Morgan, P., Bock, Y., Subarya, C., Manurung, P., Kahar, J., Abidin, H., Abu, S., 2002. Migration of seismicity and earthquake interactions monitored by GPS in SE Asia triple junction: Sulawesi, Indonesia. J. Geophys. Res. 107, 2231. doi:10.1029/2001JB000377.
Villeneuve, M., Corné, J.J., Gunawan, W., Janin, M.C., Butterlin, J., Saint-Marc, P., Samodra, H., 2000. Continental block collision in the eastern arm of Sulawesi (Indonesia). Structure and geodynamic interprétation. C. R. Acad. Sci. Paris 330, 371–378.
Walpersdorf, A., Rangin, C., Vigny, C., 1998. GPS compared to long-term geologic motion of the north arm of Sulawesi. Earth Planet. Sci. Lett. 159, 47–55.
Walpersdorf, A., Vigny, C., Subarya, C., Manurung, P., 1998. Monitoring of the Palu–Koro Fault (Sulawesi) by GPS. Geophys. Res. Lett. 25, 2313–2316.
Zhang, Y.Q., Mercier, J.L., Vergély, P., 1998. Extension in the graben systems around the Ordos (China), and its contribution to the extrusion tectonics of south China with respect to Gobi — Mongolia. Tectonophysics 285, 41–75.